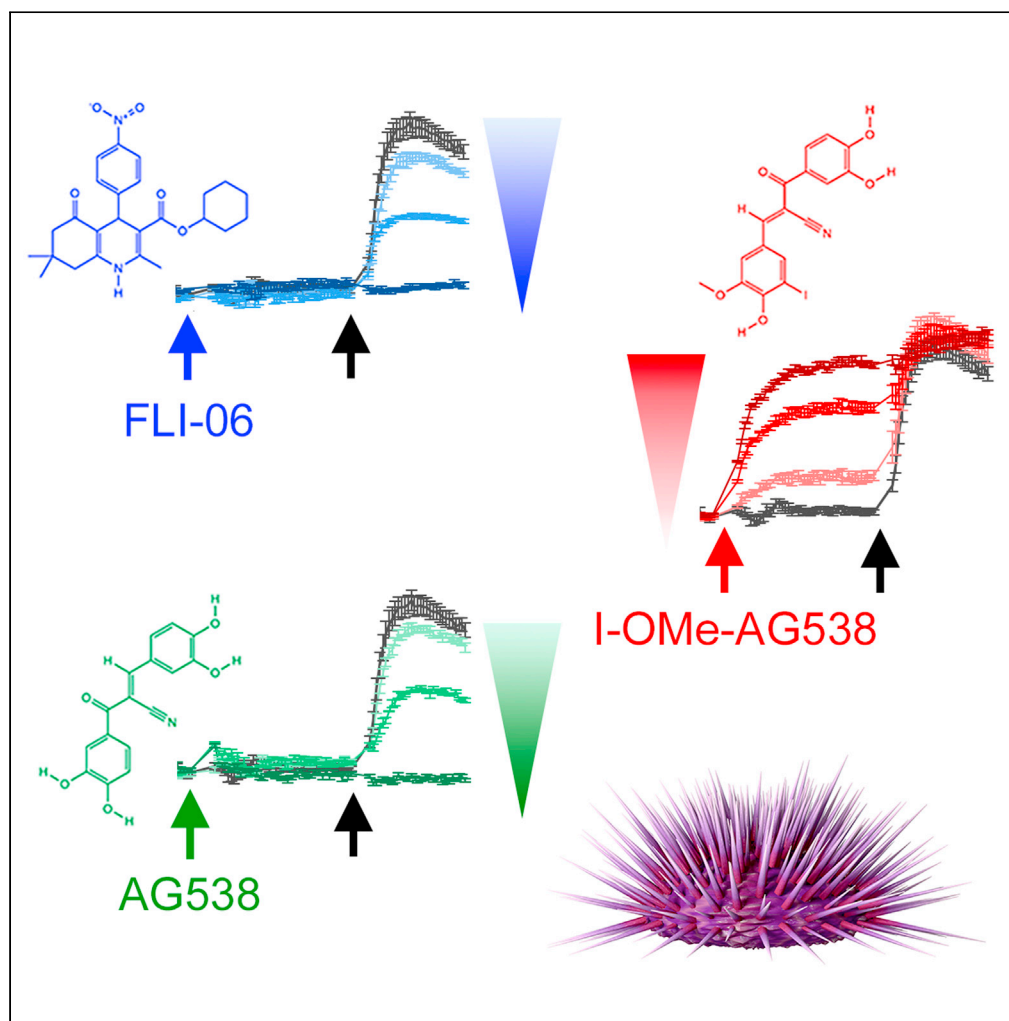


Article

Identification of a dihydropyridine scaffold that blocks ryanodine receptors



Gihan S. Gunaratne, Robyn T. Rebbeck, Lindsey M. McGurran, ..., Razvan L. Cornea, Timothy F. Walseth, Jonathan S. Marchant

jmarchant@mcw.edu

Highlights

FLI-06 inhibits transport in the secretory pathway via an unknown mechanism

An invertebrate screening platform revealed FLI-06 blocks intracellular Ca^{2+} release

FLI-06 acts as a potent, cell-permeable ryanodine receptor (RyR) blocker

The para-substituted dihydropyridine chemotype is a new scaffold for RyR modulation

Gunaratne et al., iScience 25, 103706
January 21, 2022 © 2021 The Author(s).
<https://doi.org/10.1016/j.isci.2021.103706>

Article

Identification of a dihydropyridine scaffold that blocks ryanodine receptors

Gihan S. Gunaratne,^{1,2} Robyn T. Rebbeck,³ Lindsey M. McGurran,³ Yasheng Yan,² Thiago Arzua,² Talia Frolkis,² Daniel J. Sprague,² Xiaowen Bai,² Razvan L. Cornea,³ Timothy F. Walseth,¹ and Jonathan S. Marchant^{2,4,*}

SUMMARY

Ryanodine receptors (RyRs) are large, intracellular ion channels that control Ca²⁺ release from the sarco/endoplasmic reticulum. Dysregulation of RyRs in skeletal muscle, heart, and brain has been implicated in various muscle pathologies, arrhythmia, heart failure, and Alzheimer's disease. Therefore, there is considerable interest in therapeutically targeting RyRs to normalize Ca²⁺ homeostasis in scenarios involving RyR dysfunction. Here, a simple invertebrate screening platform was used to discover new chemotypes targeting RyRs. The approach measured Ca²⁺ signals evoked by cyclic adenosine 5'-diphosphate ribose, a second messenger that sensitizes RyRs. From a 1,534-compound screen, FLI-06 (currently described as a Notch "inhibitor") was identified as a potent blocker of RyR activity. Two closely related tyrosine kinase inhibitors that stimulate and inhibit Ca²⁺ release through RyRs were also resolved. Therefore, this simple screen yielded RyR scaffolds tractable for development and revealed an unexpected linkage between RyRs and trafficking events in the early secretory pathway.

INTRODUCTION

Ryanodine receptors (RyRs) are intracellular Ca²⁺ release channels that play a critical role in excitation-contraction coupling in muscle, as well as neuronal development and homeostasis (Abu-Omar et al., 2018; Del Prete et al., 2014; Lanner, 2012). Three mammalian isoforms (RyR1–3) exist that function as large homotetramers (>2,000 kDa) localized within the sarcoplasmic/endoplasmic reticulum (ER) of cells. Dysregulation of the skeletal muscle RyR isoform (RyR1) is associated with a range of RyR1-related myopathies, encompassing clinical presentations of central core disease, malignant hypothermia, myalgias, muscular dystrophy, and sarcopenia. RyR2 dysfunction is associated with cardiac pathologies such as tachycardias and heart failure, as well as chronic neurodegenerative conditions such as Alzheimer's or Parkinson's disease. Therefore, identifying therapeutics that target aberrant RyR activity has considerable clinical relevance. This had led to efforts to optimize RyR-targeted assays for implementation in high-throughput screening (HTS) platforms. Recent HTS approaches span fluorescence resonance energy transfer-based assays between RyRs and their accessory proteins (Rebbeck et al., 2017, 2020) to whole organism-based genetic screens feeding validation pipelines (Volpatti et al., 2020).

In this brief report, we have optimized a simple screening platform that reports RyR activation by resolving the Ca²⁺-releasing ability of cyclic adenosine 5'-diphosphate ribose (cADPR), a RyR modulator. cADPR is a second messenger produced from nicotinamide adenine dinucleotide (NAD⁺) by the enzymatic action of ADP-ribosyl cyclases (ARCs). The best studied human ARC is CD38, although cADPR can be generated by other ARCs, such as CD157 and SARM1 (Essuman et al., 2017; Hirata et al., 1994; Howard et al., 1993). cADPR acts rapidly to release Ca²⁺ from intracellular Ca²⁺ stores through activation of RyRs (Lee, 2001). The precise mechanism of RyR activation by cADPR remains unclear (Venturi et al., 2012), with data suggesting an indirect interaction via one or more accessory proteins (Lee et al., 1994; Noguchi et al., 1997; Zhang et al., 2017). Dysfunction of the cADPR signaling pathway is also implicated in several diseases, including obstructive pulmonary diseases (Guedes et al., 2020), kidney injury (Shu et al., 2018), as well as inflammatory and neurodegenerative disorders (Partida-Sanchez et al., 2004; Sasaki et al., 2020; Wang et al., 2017).

To discover molecules that regulate cADPR-evoked Ca²⁺ signaling, we have carried out a screening campaign using sea urchin egg homogenate, the preparation where the Ca²⁺-releasing activity of cADPR was first discovered (Galione et al., 2014; Lee and Aarhus, 1995; Lee et al., 1993; Yuan et al., 2019). This

¹Department of Pharmacology, University of Minnesota Medical School, Minneapolis, MN 55455, USA

²Department of Cell Biology, Neurobiology and Anatomy, Medical College of Wisconsin, Milwaukee WI 53226, USA

³Department of Biochemistry, Molecular Biology and Biophysics, University of Minnesota Medical School, Minneapolis, MN 55455, USA

⁴Lead contact

*Correspondence: jmarchant@mcw.edu
<https://doi.org/10.1016/j.isci.2021.103706>



simple broken-cell system is easy to prepare and provides a robust, high signal-to-noise, room temperature assay (Lee and Aarhus, 1995; Lee et al., 1993; Yuan et al., 2019) that is amenable to miniaturization for HTS. Using this approach to screen for modulators of cADPR action, we identified new chemotypes that regulate cADPR-evoked Ca^{2+} release, with three ligands subsequently validated to act as potent, cell-permeable modulators of RyR activity in assays of mammalian and human RyRs. One of these ligands, FLI-06, is a dihydropyridine-based structure that has been previously resolved as a blocker of Notch signaling and trafficking events early in the secretory pathway in human cells (Kramer et al., 2013; Yonemura et al., 2016). FLI-06, although widely employed as a Notch “inhibitor,” lacked any defined cellular target, which we reveal here as the RyR. These outcomes evidence the utility of this simple screening platform, based on monitoring cADPR-evoked Ca^{2+} release, for the identification of novel RyR modulators.

RESULTS

A screen targeting cADPR action in sea urchin egg homogenate identifies modulators of Ca^{2+} signaling

Two commercially available chemical libraries (described in experimental methods) were used to screen for modulators of cADPR-evoked Ca^{2+} signaling in the sea urchin egg homogenate system (Galione et al., 2014; Yuan et al., 2019). Homogenate was dispensed into 96-well plates and incubated with individual test (library) compounds prior to the addition of cADPR. Fluo-3 fluorescence intensity was measured as an index of $[\text{Ca}^{2+}]$ in the homogenate preparation and was recorded before and after addition of library compound and then after addition of cADPR. In the absence of library compounds, cADPR dramatically increases Fluo-3 fluorescence intensity (Figure 1A) as previously established (Gunaratne et al., 2018). These control responses were used to calculate the Z' factor, an indicator of assay quality and readiness for HTS campaigns (Zhang et al., 1999). Using the coefficient of variance (SD/mean) and the amplitude of signal window, we determined $Z' = 0.74 \pm 0.14$ (mean \pm SD) for the miniaturized screening assay, well within the range of values ($1 > Z' \geq 0.5$) defining an assay that is ready to drive an HTS campaign.

Under these same conditions, the library compounds (1,534 total ligands) were interrogated and response data ordered by magnitude of inhibition of the amplitude of cADPR-evoked Ca^{2+} signals (Figure 1B). Although the majority of compounds fell within a $\pm 25\%$ range of control values (gray, Figure 1B), several compounds elicited strong inhibition. To examine the selectivity of the strongest “hits” against the cADPR pathway, results from the cADPR screen were cross-correlated with data from the same ligands collated in a recent screen against NAADP action, a distinct Ca^{2+} -mobilizing second messenger (Gunaratne et al., 2018). A scatter plot (Figure 1C) identified those compounds that displayed selective inhibition of cADPR- but not NAADP-evoked Ca^{2+} release (Figure 1C, upper left), or selective inhibition of NAADP- but not cADPR-evoked Ca^{2+} release (Figure 1C, bottom right). As controls for calibration, data with (1) the ionophore A23187, which inhibited cADPR- and NAADP-evoked Ca^{2+} responses (upper right, Figure 1C), and (2) thio-NADP, known to contain contaminating NAADP (Dickey et al., 1998), which selectively desensitized responses to NAADP (lower right, Figure 1C), are highlighted. The top three selective inhibitors of cADPR-evoked Ca^{2+} signals were identified as FLI-06 (Kramer et al., 2013), and two tyrosine kinase inhibitors (“tyrphostins”), AG538 and the closely related but chemically and physically distinct iodinated derivative, I-O-Me-AG538 (Figure 1D and Blum et al., 2000). To the best of our knowledge, none of these compounds has previously been shown to block cADPR action.

Secondary validation of these hits was performed after repurchasing each of these analogues and performing a full concentration-response curve analysis for blockade of cADPR-evoked Ca^{2+} release in the sea urchin egg homogenate system. These results are shown for FLI-06 (Figures 2A and 2B), AG538 (Figures 2C and 2D), and I-O-Me-AG538 (Figures 2E and 2F). Increasing concentrations of each compound progressively inhibited cADPR-evoked Ca^{2+} release but not Ca^{2+} release evoked by the distinct NAADP or IP_3 -evoked Ca^{2+} release pathways (Figures 2A, 2C, and 2E). cADPR-evoked Ca^{2+} signals were completely inhibited at concentrations that did not impact these other Ca^{2+} release pathways (Figures 2B, 2D, and 2F). FLI-06 was the most potent inhibitor of cADPR action ($\text{IC}_{50} = 260 \pm 23$ nM, Figure 2B) compared with AG538 ($\text{IC}_{50} = 1.10 \pm 0.16$ μM , Figure 2D) and I-O-Me-AG538 ($\text{IC}_{50} = 3.84 \pm 0.39$ μM , Figure 2F). Although the inhibition of cADPR action seen with FLI-06 or AG538 (≤ 100 μM) did not result from any intrinsic agonist activity associated with these two ligands, I-O-Me-AG538 elicited a concentration-dependent Ca^{2+} elevation when added to the homogenate in the absence of cADPR (Figures 2E and 2F). I-O-Me-AG538-evoked Ca^{2+} signals were sustained in profile ($\text{EC}_{50} = 9.1 \pm 1.5$ μM) and selective for cADPR-sensitive Ca^{2+} stores (Figure 2F).

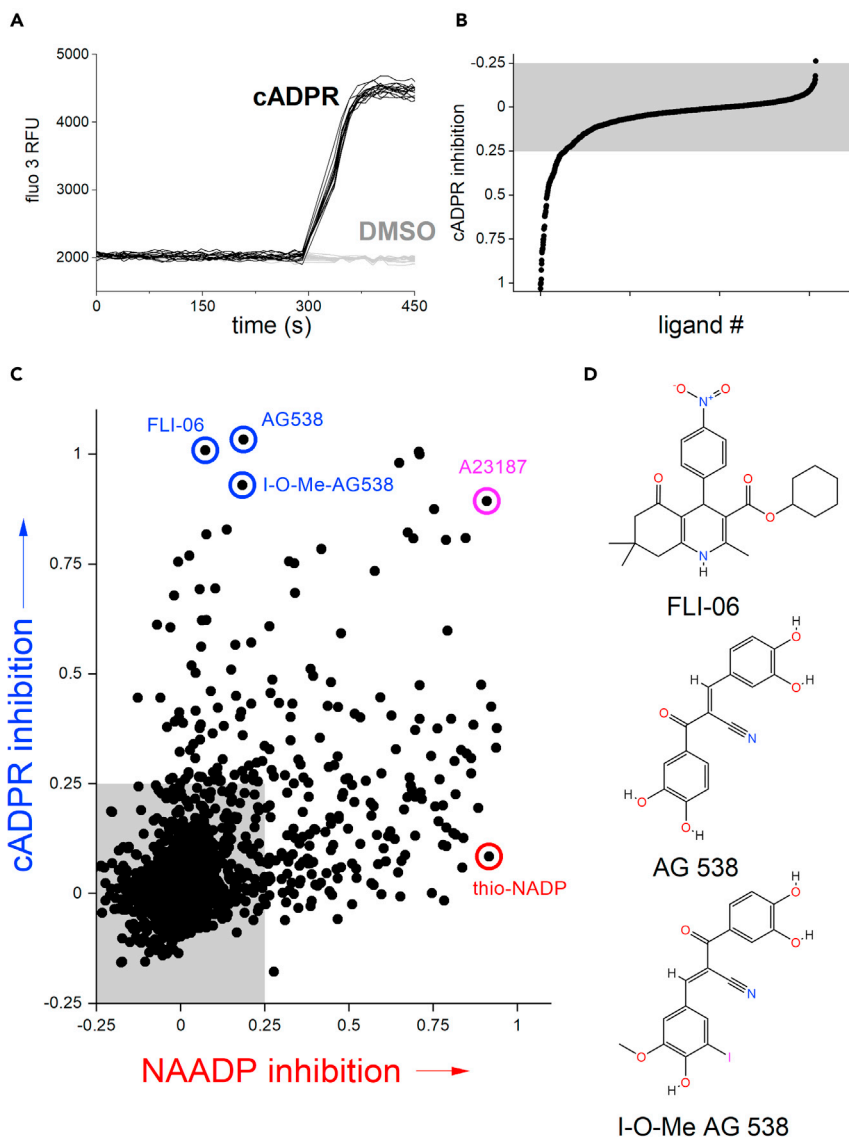


Figure 1. Primary screen to identify modulators of cADPR-evoked Ca^{2+} release

(A) Ca^{2+} release in sea urchin egg homogenate evoked by cADPR (300 nM, black) or vehicle (0.25% DMSO, gray). Changes in ambient Ca^{2+} were resolved by monitoring changes in fluo-3 fluorescence. Profiles represent fluorescence over time resolved from a single well of a 96-well plate.

(B) Plot depicting extent of inhibition of cADPR-evoked Ca^{2+} release by 1,534 compounds (single concentration, 25 μM , 6 min preincubation) ranked from greatest inhibition (rank #1, left) to potentiation (rank #1534, right). The majority of compounds were in a range $\pm 25\%$ of control response (shaded box).

(C) Scatterplot of the same dataset plotting the degree of inhibition of cADPR- (ordinate) and NAADP- (abscissa) evoked Ca^{2+} signals for each compound. Three compounds (FLI-06, AG538, I-O-Me-AG538) that selectively inhibit cADPR-evoked Ca^{2+} release (blue) are highlighted. The ionophore A23187 (magenta) and thio-NADP (red, inhibition of NAADP responses) are shown as positive controls.

(D) Chemical structures of FLI-06 (top), AG538 (middle), and I-OMe-AG538 (bottom).

The action of FLI-06 and AG538 was then compared with that of the known cADPR antagonists 8-amino-cADPR and 7-deaza-8-bromo-cADPR that are derivatized from cADPR. Increasing concentrations of either of these cADPR blockers increased the EC_{50} for cADPR-evoked Ca^{2+} release without changing the peak response to cADPR, consistent with their action as competitive inhibitors at the cADPR-binding site (Figures 2G and 2H). In contrast, increasing concentrations of FLI-06 and AG538 decreased the peak amplitude

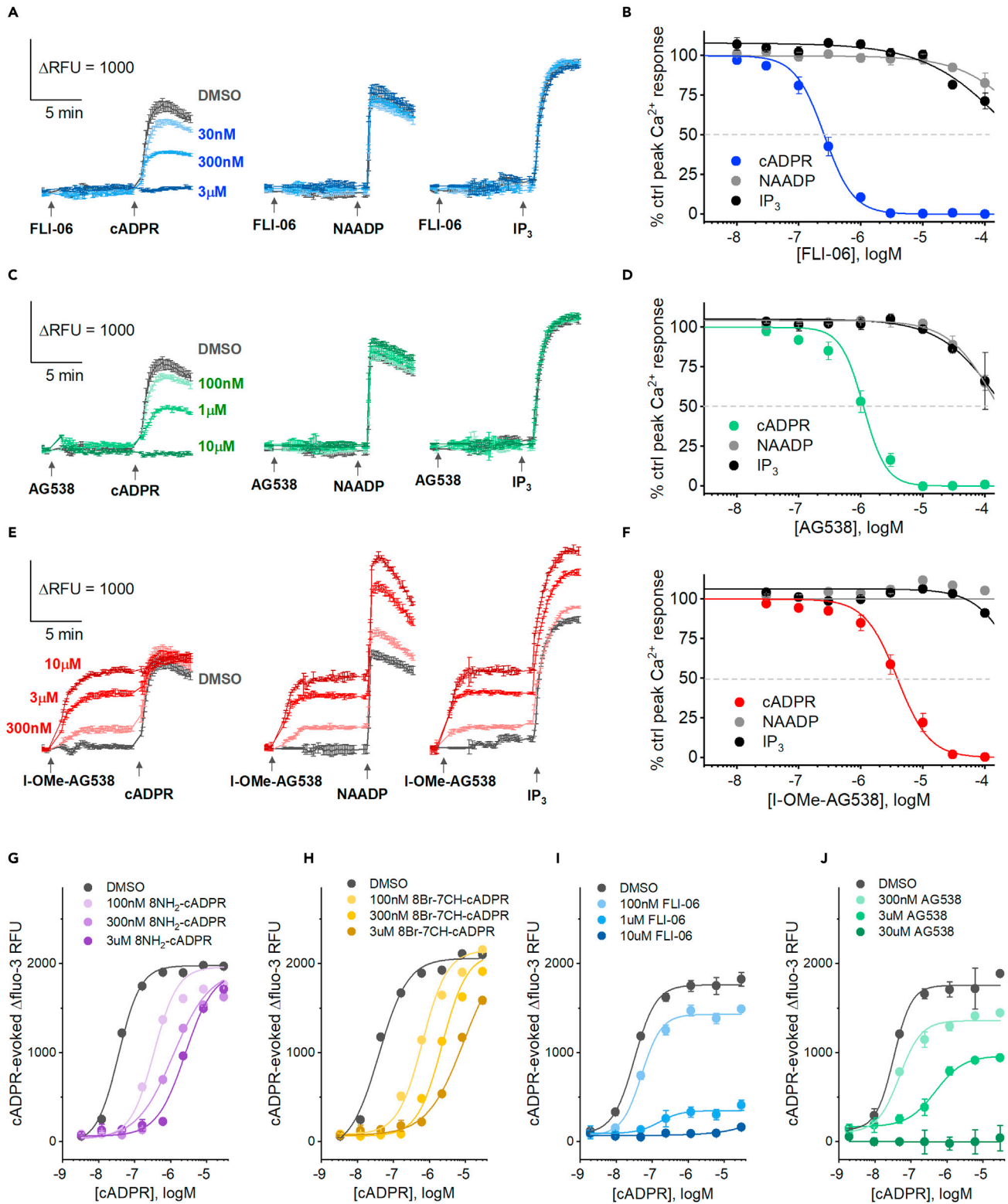


Figure 2. Secondary validation of screening hits

Effects of different concentrations of (A and B) FLI-06, (C and D) AG538, and (E and F) I-O-Me-AG538 on Ca^{2+} signals evoked by second messengers cADPR (300 nM), NAADP (200 nM), and IP_3 (500 nM). Data shown as mean \pm SEM fluo-3 fluorescence traces from a representative experiment (A, C and E) and full concentration-response curves (B, D and F) for each messenger (cADPR, NAADP, and IP_3) in the presence of each of the different compounds.

(G and H) Effects of increasing concentrations of the competitive cADPR antagonists 8-NH₂-cADPR (G) and 8Br-7-deaza-cADPR (H) on cADPR-induced Ca^{2+} release.

(I and J) Effects of increasing concentrations of FLI-06 (I) and AG538 (J) on cADPR-induced Ca^{2+} release. All concentration-response curves are calculated from mean \pm SEM values from $n = 3$ independent experiments.

and increased the EC₅₀ for cADPR action, consistent with non-competitive inhibition of cADPR action (Figures 2I and 2J).

FLI-06 inhibited cADPR signaling in human cells

Does FLI-06 also block cADPR action in human cells? To investigate this possibility, we used two independent approaches. First, we assessed the effect of FLI-06 in U2OS cells (human bone osteosarcoma), where cADPR-evoked Ca^{2+} signals are evoked by microinjection of cADPR into intact, individual cells. Single U2OS cells, expressing the genetically encoded Ca^{2+} reporter GCaMP-6M, were microinjected with intracellular buffer, or cADPR in presence of FLI-06 (5 μM), or a vehicle control (0.05% DMSO). Injection of buffer alone ("mock" injection) evoked only a small stimulus artifact, whereas injection of cADPR (30 μM pipette concentration) triggered a large Ca^{2+} signal (Figures 3A and 3B). This cADPR-evoked Ca^{2+} transient was reduced in cells preincubated with FLI-06 (5 μM , Figures 3A and 3B). Quantification of the peak amplitude (Figure 3C) and the cumulative size of these Ca^{2+} transients (Figure 3D) revealed FLI-06 inhibited endogenous cADPR-evoked Ca^{2+} signaling.

A second, orthogonal approach to study the effects of FLI-06 on cADPR action relates to the role of cADPR in cardiomyocyte differentiation (Wei et al., 2012). In mouse embryonic stem (ES) cells, endogenous cADPR-evoked Ca^{2+} signaling repressed cardiomyocyte differentiation, whereas application of the cADPR inhibitor, 8-Br-cADPR (100 μM), or knockdown of CD38 promoted the generation of cardiomyocytes (Wei et al., 2012). Here, we investigated the effects of FLI-06 on cardiomyocyte differentiation using human induced pluripotent stem cells (iPSCs) as a model. Using an established cardiomyocyte differentiation protocol (Horikoshi et al., 2019; Kikuchi et al., 2015; Lian et al., 2012), cultures that were exposed to FLI-06 (1 μM for 5 days) exhibited enhanced expression of cardiomyocyte-specific troponin T (Figure 4) and an earlier contraction phenotype compared with control cultures. Therefore, consistent with FLI-06 inhibition of cADPR action (Wei et al., 2012), low concentrations of FLI-06 accelerated human cardiomyocyte differentiation.

Action of compounds on RyRs

cADPR causes Ca^{2+} release through activation of RyRs in the sarco/endoplasmic reticulum (Lee et al., 1994; Thomas et al., 2002). To probe mechanistically how FLI-06 and AG538 inhibit cADPR action, we examined the effect of both these ligands on responses to caffeine and ryanodine, two direct activators of RyRs. cADPR structural mimetics (such as 8-NH₂-cADPR and 8-Br-7-deaza-cADPR) inhibit cADPR action, whereas they do not block caffeine- or ryanodine-evoked Ca^{2+} release (Walseth and Lee, 1993). As expected, all three compounds (FLI-06, AG538, and 8-amino-cADPR) blocked cADPR-evoked Ca^{2+} signals (Figures 5A and 5B). However, FLI-06 and AG538, but not 8-NH₂-cADPR or 8-Br-7-deaza-cADPR, also blocked caffeine- and ryanodine-evoked Ca^{2+} release (Figures 5A and 5B). These data, consistent with the observed non-competitive inhibition of cADPR activity by FLI-06 and AG538 (Figures 2I and 2J), demonstrate that FLI-06 and AG538 act as direct RyR blockers rather than competitive inhibitors of the cADPR-binding site.

To provide further insight, [³H]-ryanodine binding assays were performed, an approach routinely used to provide insight into RyR activity levels (Fruen et al., 2005). These assays were performed using preparations of sarcoplasmic reticulum (SR) vesicles isolated from either porcine heart (RyR2) or skeletal muscle (RyR1). In these assays, increasing concentrations of FLI-06 inhibited [³H]-ryanodine binding in both preparations at either relaxed (100 nM) or contracting (30 μM) free Ca^{2+} concentrations (Figure 5C). In contrast, I-O-Me-AG538 stimulated [³H]-ryanodine binding at both Ca^{2+} concentrations (Figure 5C). AG538 inhibited [³H]-ryanodine binding at high medium Ca^{2+} with little effect at resting [Ca^{2+}] (Figure 5C). The synthetically tractable differences in compound structure (Figure 1D) that manifest as agonism (I-O-Me-AG538) or

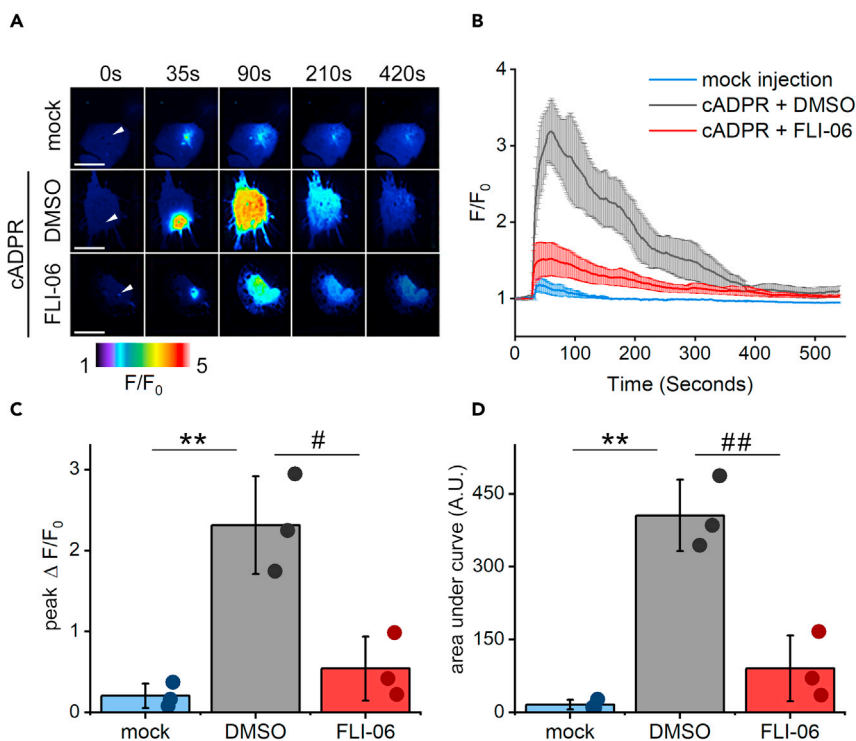


Figure 3. Effect of FLI-06 on cADPR-evoked Ca^{2+} signals in a human cell line

(A) Pseudocolor image of individual U2OS cells expressing GCaMP6M, imaged in Ca^{2+} -free HBSS. Images are captured at different time points from cells injected with either intracellular buffer ("mock injection") or cADPR (~300 nM intracellular concentration) in the presence of DMSO (0.05%) or FLI-06 (5 μM). Scale bar represents 10 μm , arrows indicate injection sites.

(B) Traces of mean \pm SD changes in GCaMP6M fluorescence from three independent microinjections for each condition. (C and D) Bar graphs for peak F/F_0 (C) and area under the curve (D) represent mean \pm SD values taken from $n = 3$ independent sets of injections. ** $p < 0.01$ versus mock injection, # $p < 0.05$ and ## $p < 0.01$ versus cADPR injection in the presence of DMSO using the Student's t test.

antagonism at RyRs (AG538) are encouraging for structure-activity relationship (SAR) studies focused on this chemical scaffold. Furthermore, these [^3H]-ryanodine binding data for the three compounds are consistent with the functional data from the sea urchin system (two inhibitors, one activator), although the observed potencies in [^3H]-ryanodine assays in membrane vesicles were lower than those seen with functional assays in sea urchin egg homogenate (Figure 2) or human cell microinjection experiments (Figure 3). cADPR did not elicit any effects on [^3H]-ryanodine binding in these SR preparations (Figure 5C).

Screening of FLI-06 derivatives

FLI-06 was originally identified as an inhibitor of intracellular secretory traffic that caused accumulation of a Notch trafficking reporter within ER membranes (Kramer et al., 2013; Yonemura et al., 2016). We therefore compared the ability of FLI-06 to inhibit Notch reporter trafficking (Kramer et al., 2013; Yonemura et al., 2016) with block of cADPR-evoked Ca^{2+} signaling. This was done via an SAR "by catalog" approach using 15 purchased analogues (Table S1). This catalog search yielded ligands that altered the sterics and/or electronics of the ester (at the 3-position of the DHP) as well as the aryl ring (at the 4-position of the DHP). Across the series of 15 derivatives, inhibition of both phenotypes (secretory trafficking, cADPR-evoked Ca^{2+} release) was correlated: analogues that more potently blocked cADPR action caused a greater inhibition of Notch trafficking (Figure 6). The observed blockade of cADPR-evoked Ca^{2+} release occurred at lower concentrations than the effects of FLI-06 on secretory trafficking ($\text{EC}_{50} = 153 \pm 26$ nM for inhibition of cADPR action versus $\text{EC}_{50} = 2.3$ μM for inhibition of notch trafficking [Gomez-Galeno et al., 2018; Kramer et al., 2013]). Screened analogues clustered into groups of high (green), intermediate (orange), and low potency (red, Figure 6). Several trends were identified from the SAR analysis.

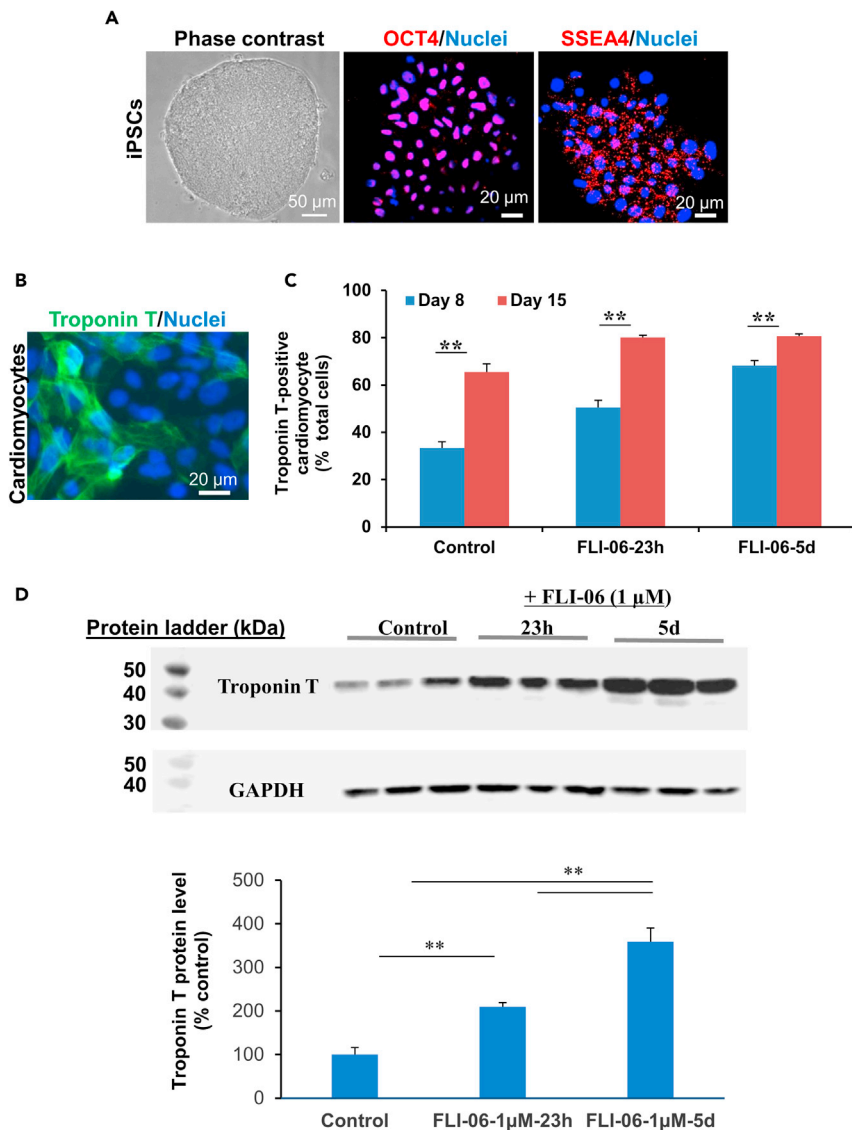


Figure 4. Effects of FLI-06 on induced pluripotent stem cell differentiation into cardiomyocytes

(A) Characterization of iPSCs. Left, phase contrast image of iPSC growth as colonies. These iPSC colonies were shown to express pluripotent stem cell-specific markers OCT4 (middle) and stage-specific embryonic antigen-4 (SSEA4, right) by immunofluorescence. Cell nuclei are stained with Hoechst 33342.

(B) iPSC colonies were induced to differentiate into a cardiomyocyte fate using a protocol lasting ~2 weeks (see methods). Expression of the cardiac-specific marker troponin T (green) is evident at day 8 after initiation of differentiation in control cultures. All cultures displayed a contractile phenotype after 12 days of culture.

(C) Quantification of immunofluorescence staining (as performed in (B)) to resolve the effect of FLI-06 on cardiomyocyte differentiation. The differentiation culture was treated with FLI-06 (1 μ M) at day 0 for either 23 h or 5 days. Troponin T-positive cardiomyocytes were counted after 8 or 15 days of differentiation. FLI-06-treated cultures displayed more rapid expression of troponin T and spontaneous contractions were also observed earlier (by day 10) than seen with control cultures. Data are presented as mean \pm SD, n = 3, **p < 0.01 by Student's t test.

(D) *Top*, western blot of the effect of FLI-06 on troponin T expression. *Bottom*, densitometry analysis of results. Troponin T expression was normalized to the endogenous control glyceraldehyde 3-phosphate dehydrogenase (GAPDH). n = 3, **p < 0.01. One-way ANOVA and Tukey test were used for comparison between multiple groups.

First, these assays identified a compound #8 (FLI-28), an FLI-06 derivative with a cycloheptyl substitution (Kramer et al., 2013), that was considerably more potent (IC₅₀ = 61 \pm 14 nM) than FLI-06 at inhibiting CADPR-evoked Ca²⁺ release (Figure 6). FLI-28 was also the most potent inhibitor of Notch reporter

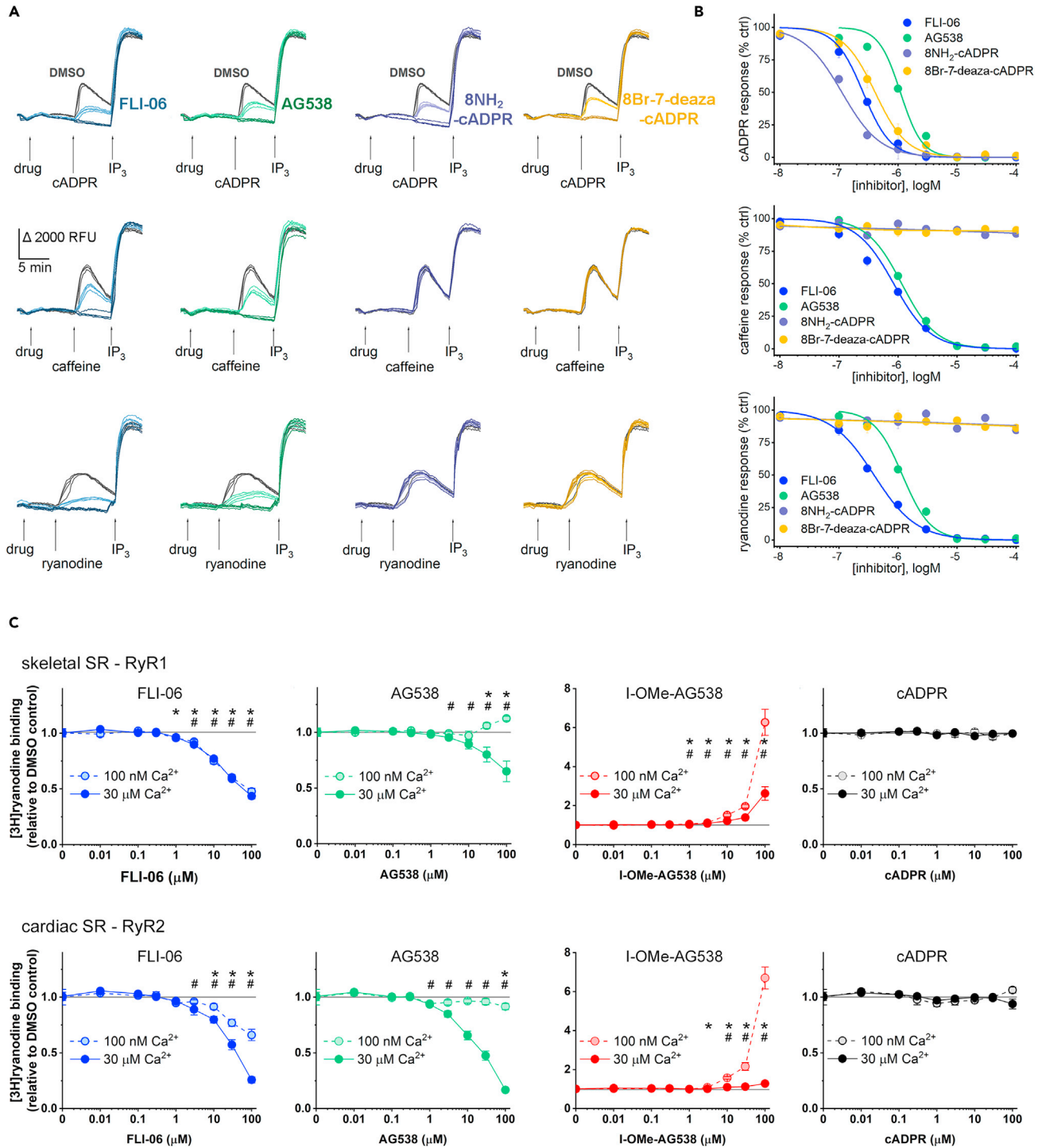


Figure 5. Action of compounds as RyR modulators using sea urchin homogenate or porcine muscle SR membrane

(A) Effects of increasing concentrations of FLI-06 (blue), AG538 (green), 8-NH₂-cADPR (purple), and 8Br-7-deaza-cADPR (yellow) on cADPR-evoked (300 nM, top), caffeine-evoked (15 mM, middle), or ryanodine-evoked (100 μM, bottom) Ca²⁺ release in sea urchin egg homogenate. Responses to IP₃ (500 nM) were unaffected. Data shown as four individual fluo-3 fluorescence traces per condition from a representative experiment.

(B) Concentration-response curves showing effects of each of the four compounds on responses to cADPR (top), caffeine (middle), and ryanodine (lower). Data are shown as mean ± SEM from *n* = 3 independent biological experiments.

Figure 5. Continued

(C) Effects of FLI-06, AG538, l-O-Me-AG538, and cADPR on [³H]-ryanodine binding to skeletal (top) and cardiac (bottom) SR vesicles measured at relaxed (100 nM [Ca²⁺], open circles) and contracting (30 μM [Ca²⁺], solid circles). Data are shown as mean ± SEM values from n ≥ 4 independent biological experiments. *p < 0.05, 100 nM [Ca²⁺] versus DMSO controls; #p < 0.05, 30 μM [Ca²⁺] versus DMSO controls using the Student's t test.

trafficking (Figure 6, Kramer et al., 2013). However, in contrast to the favorable effects of steric bulk of the ester (cycloheptyl versus cyclohexyl), linear expansion of the ester was not tolerated, as compounds #9 and #11 displayed decreased potency.

Second, the most active compounds contain electron-deficient substituents at the 4-position of the aryl substituent (Table S1, green grouping in Figure 6). This was evident in FLI-06 (4-NO₂-Ph), as well as compounds #8 (FLI-28, 4-NO₂-Ph), #2 (4-Br-Ph), and #5 (4-Cl-Ph). As the electron density increased, a trend of decreased potency emerged. Compounds #13 (4-OMe-Ph) and #1 (4-H-Ph) displayed intermediate potency. Further increases in electron density of the ring (compounds #3 (4-OH-Ph), #6 (3-OH-Ph), and #4 (4-Me₂N-Ph) resulted in low-potency analogues. Although compound #15 (4-AcO-Ph) clustered within the low-potency group of analogues despite containing an electron-withdrawing group at the aryl ring 4-position, this analogue is likely cleaved to the free phenol-yielding compound #3.

Finally, different substitutions around the aryl ring were less tolerated. Compounds #12 (3-F-Ph) and #14 (3-Br-Ph) despite containing an electron-withdrawing group exhibited decreased potency. Compounds #7 (4-NO₂-Ph) and #14 (3-Br-Ph) differ solely in their substitution pattern on the aromatic ring. Compound #14 displayed low potency, whereas #7 had intermediate potency (with the loss of potency compared with FLI-06 attributed to the linear expansion of the ester change as discussed above).

DISCUSSION

Here we have identified two novel RyR inhibitors (FLI-06 and AG-538) and one RyR activator (l-O-Me-AG538) that represent novel chemotypes that modulate RyR activity. The most potent inhibitor identified in the screen was FLI-06, which inhibited RyR activation by cADPR, caffeine, or ryanodine. Further SAR afforded FLI-28, compound #8, as a more potent analogue. Structurally, these compounds are annulated dihydropyridines, containing the 1,4-dihydropyridine (DHP) scaffold found in many bioactive molecules (Figure 1D), but best known as the core of a class of voltage-operated calcium channel (Ca_v) blockers (Bosert and Vater, 1971). However, FLI-06 is structurally distinct from DHPs that act as Ca_v blockers: FLI-06 contains a *para*-substituted phenyl group at the 4-position of the DHP (Figure 1D) compared with an *ortho*-substituted phenyl group (nifedipine, Table S1) or a *meta*-substituted phenyl group (nimodipine, Table S1) that are both pore blockers of cell surface Ca_v channels. The 1,4-DHPs that act on cell surface Ca_v channels do not block RyRs (Yusufi et al., 2002): for example, both nimodipine and nifedipine were present in the LOPAC library screened here and neither inhibited cADPR-evoked Ca²⁺ signals (inhibition was ~5% and ~3% at 25 μM, respectively). This was unsurprising as both these DHPs demonstrate multiple "red flags" in regard to the SAR trends identified in the results section. Neither contain an electron-withdrawing (or halogen) substitution at the 4-position of the aryl ring, which proved crucial for RyR engagement. Both nimodipine and nifedipine also have unfavorable ester properties. Nimodipine contains a methoxyethyl ester, which resembles the unfavorable long chains resolved from the SAR-by-catalog. In this regard, nifedipine resembles compound #10, which contains a methyl ester. Finally, neither nimodipine nor nifedipine is annulated. Overall, in terms of cellular action, the exclusion of a "Ca²⁺ hypothesis" for FLI-06 action based on a lack of effect of DHPs that act on cell surface Ca_vs (Kramer et al., 2013) overlooked a possible action of this (different) class of DHPs against intracellular Ca²⁺ channels, which exhibit different SAR requirements.

Here, we unmask RyRs as the likely intracellular target of FLI-06. As a potent, cell-permeable RyR blocker, FLI-06 provides a new tool for manipulating RyR activity in cells, and the identification of a more potent RyR-blocking derivative, FLI-28 (Figure 6), suggests iterations of this core structure may yet yield even more potent ligands. Given the involvement of RyRs in a variety of disease states (Lanner, 2012; Liang and Wei, 2015), further evaluation of these tools is merited. We note that FLI-06 was originally identified as a blocker of secretory trafficking (by following the processing of a GFP-tagged Notch reporter) in mammalian cells (Kramer et al., 2013; Yonemura et al., 2016). Chronic FLI-06 treatment disperses the Golgi apparatus by disrupting transport through the secretory pathway (Kramer et al., 2013; Yonemura et al., 2016). Identification of FLI-06 as a RyR blocker implicates RyRs as mediators of the phenotypic action of FLI-06, as

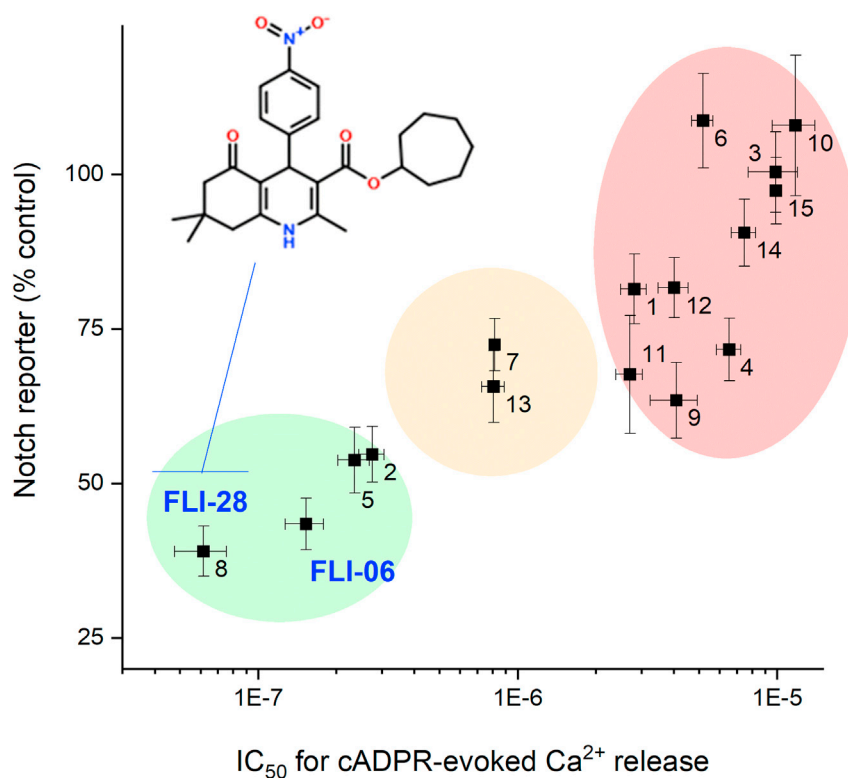


Figure 6. FLI-06 analogues modulate cADPR-evoked Ca²⁺ signaling and Notch reporter trafficking

Correlation between cADPR-evoked Ca²⁺ release (IC₅₀ in the sea urchin egg homogenate system, mean ± SEM) and inhibition of Notch trafficking (% control luminescence values in HEK293 cells after incubation with 10 μM analogue for 24 h, mean ± SEM) across a series of 15 FLI-06 derivatives. The structure of analogue “8” known as FLI-28 is highlighted as the most potent inhibitor of both cADPR-evoked Ca²⁺ release and Notch trafficking. Identity of FLI-06 analogs is detailed in Table S1. Data are clustered into groups of high- (green), intermediate- (orange), and low- (red) potency analogues to facilitate discussion of SAR trends. Values are from n ≥ 4 independent biological experiments.

supported by the correlation between effects on Notch reporter trafficking and cADPR-evoked Ca²⁺ signaling (Figure 6). FLI-06 has been shown to rapidly block cargo recruitment at ER exit sites (ERESs), specialized ER regions that orchestrate transport of proteins from the ER to the Golgi apparatus (Yonemura et al., 2016). However, the molecular target of FLI-06 at the level of the ER was previously unknown (Kramer et al., 2013; Yonemura et al., 2016). Having now implicated the RyR, it is relevant to note that Ca²⁺ has long been recognized as an essential regulator of trafficking from the ER to the Golgi (Beckers and Balch, 1989), engaging a variety of Ca²⁺ sensors (annexin A11, ALG-2) that stabilize coat protein complex II (COPII) components at ER exit sites (Bentley et al., 2010; Maki et al., 2016; Shibata et al., 2015). These Ca²⁺ changes controlling secretory traffic may well be agonist dependent, coupling cell stimulation to changes in secretory flux. Further investigation of the relationship between RyR activity and ERES function is warranted based on this new insight.

The other chemotype discovered in our screen was represented by the tyrphostin ligands (AG538 and I-O-Me-AG538). AG538 was originally identified as a potent inhibitor of the insulin growth factor-1 receptor (IGF-1R) kinase domain by acting as a competitive substrate inhibitor (Blum et al., 2000). Both AG538 and I-O-Me-AG538 also inhibit other kinases over higher concentration ranges via different mechanisms (Blum et al., 2000; Davis et al., 2013). Our data support an even broader polypharmacology underscoring the need for caution when ascribing functional effects to a particular mechanism, especially if drugs are being used at concentrations exceeding their effective concentration range on individual targets. What is particularly noteworthy with these two analogues is how the addition of an iodine atom (Figure 1D) interconverts between agonism (I-O-Me-AG538) and antagonism (AG538) of the RyR complex. The increased hydrophobicity or size afforded by the iodine atom potentially endows I-O-Me-AG538 with enhanced

interactions within the RyR complex favoring channel opening. Alternatively, the iodine atom may enable halogen bonding to induce a receptor conformation favoring agonism. As the exact binding pocket and poise of these molecules is unknown, it is unfruitful to speculate further. Further work to elucidate their mode of action on the RyR complex is needed.

In conclusion, we report the discovery of two new chemotypes that act as potent, cell permeable, RyR modulators by screening for modulators of cADPR action. All three compounds were identified from a small screening campaign in sea urchin egg homogenate, highlighting the potential of this simple invertebrate model system for discovering new tools that manipulate intracellular Ca^{2+} signaling. A brief SAR-by-catalog was performed that highlights the potential for further optimization of these ligands to identify derivatives suitable for manipulating RyR behavior in various scenarios of health and disease.

Limitations of study

This study reports a primary screen and secondary validation of ligands that act as agonists (l-O-Me-AG538) or antagonists (FLI-06, AG538) of Ca^{2+} release through ryanodine receptors. Further work will be needed to define the binding sites of each of these ligands on ryanodine receptors, or potentially RyR-associated accessory proteins. Electrophysiological or radioligand binding assays utilizing purified or reconstituted RyRs could yield this information. Second, although this small, foundational screen (1,534 compounds) uncovered several unrecognized modulators of RyR-mediated Ca^{2+} release, these did not work through modulating cADPR action. This was the intent of the original screen. Likely, a larger screening campaign would be needed, coupled with additional counterscreening using caffeine to prioritize chemotypes that regulate cADPR action.

STAR★METHODS

Detailed methods are provided in the online version of this paper and include the following:

- KEY RESOURCES TABLE
- RESOURCE AVAILABILITY
 - Lead contact
 - Materials availability
 - Data and code availability
- EXPERIMENTAL MODEL AND SUBJECT DETAILS
 - Cell lines
 - Cell-free systems
- METHOD DETAILS
 - Drugs and molecular reagents
 - Chemical syntheses
 - Ca^{2+} flux assays in sea urchin egg homogenate
 - Mammalian cell microinjection
 - [^3H]-ryanodine binding to SR vesicles
- QUANTIFICATION AND STATISTICAL ANALYSIS

SUPPLEMENTAL INFORMATION

Supplemental information can be found online at <https://doi.org/10.1016/j.isci.2021.103706>.

ACKNOWLEDGMENTS

This work was supported by NIH GM088790 (to J.S.M.) and HL138539 (to R.L.C.).

AUTHOR CONTRIBUTIONS

G.S.G., R.T.R., L.M.M., Y.Y., T.A., T.F., and D.J.S. acquired data and interpreted results. G.S.G. and J.S.M. prepared the manuscript draft. G.S.G., R.T.R., Y.Y., X.B., R.L.C., T.F.W., and J.S.M. reviewed and edited the manuscript. All authors have read and agreed to publish the submitted manuscript.

DECLARATION OF INTERESTS

RLC holds equity in and serves as an executive officer for Photonic Pharma LLC. This relationship has been reviewed and managed by the University of Minnesota. Photonic Pharma had no role in this study, except to

provide access to instrumentation. G.S.G., R.T.R., L.M.M., Y.Y., T.A., T.F., D.J.S., X.B., T.F.W., and J.S.M. have no conflicts of interest to disclose.

INCLUSION AND DIVERSITY

One or more of the authors of this paper self-identifies as a member of the LGBTQ+ community. One or more of the authors of this paper self-identifies as living with a disability.

Received: September 9, 2021

Revised: November 16, 2021

Accepted: December 23, 2021

Published: January 21, 2022

REFERENCES

- Abu-Omar, N., Das, J., Szeto, V., and Feng, Z.P. (2018). Neuronal ryanodine receptors in development and aging. *Mol. Neurobiol.* 55, 1183–1192.
- Beckers, C.J., and Balch, W.E. (1989). Calcium and GTP: essential components in vesicular trafficking between the endoplasmic reticulum and Golgi apparatus. *J. Cell Biol.* 108, 1245–1256.
- Bentley, M., Nycz, D.C., Joglekar, A., Fertschai, I., Malli, R., Graier, W.F., and Hay, J.C. (2010). Vesicular calcium regulates coat retention, fusogenicity, and size of pre-Golgi intermediates. *Mol. Biol. Cell* 21, 1033–1046.
- Blum, G., Gazit, A., and Levitzki, A. (2000). Substrate competitive inhibitors of IGF-1 receptor kinase. *Biochemistry (Moscow)* 39, 15705–15712.
- Bossert, F., and Vater, W. (1971). [Dihydropyridines, a new group of strongly effective coronary therapeutic agents]. *Naturwissenschaften* 58, 578.
- Chen, T.W., Wardill, T.J., Sun, Y., Pulver, S.R., Renninger, S.L., Baohan, A., Schreier, E.R., Kerr, R.A., Orger, M.B., Jayaraman, V., et al. (2013). Ultrasensitive fluorescent proteins for imaging neuronal activity. *Nature* 499, 295–300.
- Clapper, D.L., Walseth, T.F., Dargie, P.J., and Lee, H.C. (1987). Pyridine nucleotide metabolites stimulate calcium release from sea urchin egg microsomes desensitized to inositol trisphosphate. *J. Biol. Chem.* 262, 9561–9568.
- Davis, M.I., Sasaki, A.T., Shen, M., Emerling, B.M., Thorne, N., Michael, S., Pragani, R., Boxer, M., Sumita, K., Takeuchi, K., et al. (2013). A homogeneous, high-throughput assay for phosphatidylinositol 5-phosphate 4-kinase with a novel, rapid substrate preparation. *PLoS One* 8, e54127.
- Del Prete, D., Checler, F., and Chami, M. (2014). Ryanodine receptors: physiological function and deregulation in Alzheimer disease. *Mol. Neurodegener* 9, 21.
- Dickey, D.M., Aarhus, R., Walseth, T.F., and Lee, H.C. (1998). Thio-NADP is not an antagonist of NAADP. *Cell Biochem. Biophys.* 28, 63–73.
- Essuman, K., Summers, D.W., Sasaki, Y., Mao, X., DiAntonio, A., and Milbrandt, J. (2017). The SARM1 toll/interleukin-1 receptor domain possesses intrinsic NAD(+) cleavage activity that promotes pathological axonal degeneration. *Neuron* 93, 1334–1343 e1335.
- Fruen, B.R., Balog, E.M., Schafer, J., Nitu, F.R., Thomas, D.D., and Cornea, R.L. (2005). Direct detection of calmodulin tuning by ryanodine receptor channel targets using a Ca²⁺-sensitive acrylodan-labeled calmodulin. *Biochemistry (Moscow)* 44, 278–284.
- Fruen, B.R., Bardy, J.M., Byrem, T.M., Strasburg, G.M., and Louis, C.F. (2000). Differential Ca²⁺ sensitivity of skeletal and cardiac muscle ryanodine receptors in the presence of calmodulin. *Am. J. Physiol. Cell Physiol* 279, C724–C733.
- Galione, A., Chuang, K.T., Funnell, T.M., Davis, L.C., Morgan, A.J., Ruas, M., Parrington, J., and Churchill, G.C. (2014). Preparation and use of sea urchin egg homogenates for studying NAADP-mediated Ca²⁺(+) release. *Cold Spring Harb Protoc.* 2014, 988–992.
- Gomez-Galeno, J.E., Hurtado, C., Cheng, J., Yardimci, C., Mercola, M., and Cashman, J.R. (2018). b-Annulated 1,4-dihydropyridines as Notch inhibitors. *Bioorg. Med. Chem. Lett.* 28, 3363–3367.
- Guedes, A.G., Dileepan, M., Jude, J.A., Deshpande, D.A., Walseth, T.F., and Kannan, M.S. (2020). Role of CD38/cADPR signaling in obstructive pulmonary diseases. *Curr. Opin. Pharmacol.* 51, 29–33.
- Gunaratne, G.S., Johns, M.E., Hintz, H.M., Walseth, T.F., and Marchant, J.S. (2018). A screening campaign in sea urchin egg homogenate as a platform for discovering modulators of NAADP-dependent Ca²⁺ signaling in human cells. *Cell Calcium* 75, 42–52.
- Hirata, Y., Kimura, N., Sato, K., Ohsugi, Y., Takasawa, S., Okamoto, H., Ishikawa, J., Kaisho, T., Ishihara, K., and Hirano, T. (1994). ADP-ribosyl cyclase activity of a novel bone marrow stromal cell surface molecule, BST-1. *FEBS Lett.* 356, 244–248.
- Horikoshi, Y., Yan, Y., Terashvili, M., Wells, C., Horikoshi, H., Fujita, S., Bosnjak, Z.J., and Bai, X. (2019). Fatty acid-treated induced pluripotent stem cell-derived human cardiomyocytes exhibit adult cardiomyocyte-like energy metabolism phenotypes. *Cells* 8, 1095.
- Howard, M., Grimaldi, J.C., Bazan, J.F., Lund, F.E., Santos-Argumedo, L., Parkhouse, R.M., Walseth, T.F., and Lee, H.C. (1993). Formation and hydrolysis of cyclic ADP-ribose catalyzed by lymphocyte antigen CD38. *Science* 262, 1056–1059.
- Jain, P., Slama, J.T., Perez-Haddock, L.A., and Walseth, T.F. (2010). Nicotinic acid adenine dinucleotide phosphate analogues containing substituted nicotinic acid: effect of modification on Ca²⁺ release. *J. Med. Chem.* 53, 7599–7612.
- Kikuchi, C., Bienengraeber, M., Canfield, S., Koopmeiner, A., Schafer, R., Bosnjak, Z.J., and Bai, X. (2015). Comparison of cardiomyocyte differentiation potential between type 1 diabetic donor- and nondiabetic donor-derived induced pluripotent stem cells. *Cell Transpl.* 24, 2491–2504.
- Kramer, A., Mentrup, T., Kleizen, B., Rivera-Milla, E., Reichenbach, D., Enzensperger, C., Nohl, R., Tauscher, E., Gorus, H., Ploubidou, A., et al. (2013). Small molecules intercept Notch signaling and the early secretory pathway. *Nat. Chem. Biol.* 9, 731–738.
- Lanner, J.T. (2012). Ryanodine receptor physiology and its role in disease. *Adv. Exp. Med. Biol.* 740, 217–234.
- Lee, H.C. (2001). Physiological functions of cyclic ADP-ribose and NAADP as calcium messengers. *Annu. Rev. Pharmacol. Toxicol.* 41, 317–345.
- Lee, H.C., and Aarhus, R. (1995). A derivative of NADP mobilizes calcium stores insensitive to inositol trisphosphate and cyclic ADP-ribose. *J. Biol. Chem.* 270, 2152–2157.
- Lee, H.C., Aarhus, R., Graeff, R., Gurnack, M.E., and Walseth, T.F. (1994). Cyclic ADP-ribose activation of the ryanodine receptor is mediated by calmodulin. *Nature* 370, 307–309.
- Lee, H.C., Aarhus, R., and Walseth, T.F. (1993). Calcium mobilization by dual receptors during fertilization of sea urchin eggs. *Science* 261, 352–355.
- Lian, X., Hsiao, C., Wilson, G., Zhu, K., Hazeltine, L.B., Azarin, S.M., Raval, K.K., Zhang, J., Kamp, T.J., and Palecek, S.P. (2012). Robust cardiomyocyte differentiation from human pluripotent stem cells via temporal modulation of canonical Wnt signaling. *Proc. Natl. Acad. Sci. U. S. A.* 109, E1848–E1857.

- Liang, L., and Wei, H. (2015). Dantrolene, a treatment for Alzheimer disease? *Alzheimer Dis. Assoc. Disord.* *29*, 1–5.
- Maki, M., Takahara, T., and Shibata, H. (2016). Multifaceted roles of ALG-2 in Ca²⁺-regulated membrane trafficking. *Int. J. Mol. Sci.* *17*, 1401.
- Noguchi, N., Takasawa, S., Nata, K., Tohgo, A., Kato, I., Ikehata, F., Yonekura, H., and Okamoto, H. (1997). Cyclic ADP-ribose binds to FK506-binding protein 12.6 to release Ca²⁺ from islet microsomes. *J. Biol. Chem.* *272*, 3133–3136.
- Partida-Sanchez, S., Iribarren, P., Moreno-Garcia, M.E., Gao, J.L., Murphy, P.M., Oppenheimer, N., Wang, J.M., and Lund, F.E. (2004). Chemotaxis and calcium responses of phagocytes to formyl peptide receptor ligands is differentially regulated by cyclic ADP ribose. *J. Immunol.* *172*, 1896–1906.
- Rebbeck, R.T., Essawy, M.M., Nitu, F.R., Grant, B.D., Gillispie, G.D., Thomas, D.D., Bers, D.M., and Cornea, R.L. (2017). High-throughput screens to discover small-molecule modulators of ryanodine receptor calcium release channels. *SLAS Discov.* *22*, 176–186.
- Rebbeck, R.T., Singh, D.P., Janicek, K.A., Bers, D.M., Thomas, D.D., Launikonis, B.S., and Cornea, R.L. (2020). RyR1-targeted drug discovery pipeline integrating FRET-based high-throughput screening and human myofiber dynamic Ca²⁺ assays. *Scientific Rep.* *10*, 1791.
- Sasaki, Y., Engber, T.M., Hughes, R.O., Figley, M.D., Wu, T., Bosanac, T., Devraj, R., Milbrandt, J., Krauss, R., and DiAntonio, A. (2020). cADPR is a gene dosage-sensitive biomarker of SARM1 activity in healthy, compromised, and degenerating axons. *Exp. Neurol.* *329*, 113252.
- Shibata, H., Kanadome, T., Sugiura, H., Yokoyama, T., Yamamuro, M., Moss, S.E., and Maki, M. (2015). A new role for annexin A11 in the early secretory pathway via stabilizing Sec31A protein at the endoplasmic reticulum exit sites (ERES). *J. Biol. Chem.* *290*, 4981–4993.
- Shu, B., Feng, Y., Gui, Y., Lu, Q., Wei, W., Xue, X., Sun, X., He, W., Yang, J., and Dai, C. (2018). Blockade of CD38 diminishes lipopolysaccharide-induced macrophage classical activation and acute kidney injury involving NF-kappaB signaling suppression. *Cell. Signal.* *42*, 249–258.
- Thomas, J.M., Summerhill, R.J., Fruen, B.R., Churchill, G.C., and Galione, A. (2002). Calmodulin dissociation mediates desensitization of the cADPR-induced Ca²⁺ release mechanism. *Curr. Biol.* *12*, 2018–2022.
- Venturi, E., Pitt, S., Galfre, E., and Sitsapesan, R. (2012). From eggs to hearts: what is the link between cyclic ADP-ribose and ryanodine receptors? *Cardiovasc. Ther.* *30*, 109–116.
- Volpatti, J.R., Endo, Y., Knox, J., Groom, L., Brennan, S., Noche, R., Zuercher, W.J., Roy, P., Dirksen, R.T., and Dowling, J.J. (2020). Identification of drug modifiers for RYR1-related myopathy using a multi-species discovery pipeline. *eLife* *9*, e52946.
- Walseth, T.F., and Lee, H.C. (1993). Synthesis and characterization of antagonists of cyclic-ADP-ribose-induced Ca²⁺ release. *Biochim. Biophys. Acta* *1178*, 235–242.
- Walseth, T.F., Lin-Moshier, Y., Jain, P., Ruas, M., Parrington, J., Galione, A., Marchant, J.S., and Slama, J.T. (2012). Photoaffinity labeling of high affinity nicotinic acid adenine dinucleotide phosphate (NAADP)-binding proteins in sea urchin egg. *J. Biol. Chem.* *287*, 2308–2315.
- Wang, Y.M., Liu, Z.Y., Ai, Y.H., Zhang, L.N., Zou, Y., and Peng, Q.Y. (2017). Blocking the CD38/cADPR pathway plays a double-edged role in LPS stimulated microglia. *Neuroscience* *361*, 34–42.
- Wei, W.J., Sun, H.Y., Ting, K.Y., Zhang, L.H., Lee, H.C., Li, G.R., and Yue, J. (2012). Inhibition of cardiomyocytes differentiation of mouse embryonic stem cells by CD38/cADPR/Ca²⁺ signaling pathway. *J. Biol. Chem.* *287*, 35599–35611.
- Yonemura, Y., Li, X., Muller, K., Kramer, A., Atigbire, P., Mentrup, T., Feuerhake, T., Kroll, T., Shomron, O., Nohl, R., et al. (2016). Inhibition of cargo export at ER exit sites and the trans-Golgi network by the secretion inhibitor FLI-06. *J. Cell Sci.* *129*, 3868–3877.
- Yuan, Y., Gunaratne, G.S., Marchant, J.S., and Patel, S. (2019). Probing Ca²⁺ release mechanisms using sea urchin egg homogenates. *Methods Cell Biol.* *151*, 445–458.
- Yusufi, A.N., Cheng, J., Thompson, M.A., Burnett, J.C., and Grande, J.P. (2002). Differential mechanisms of Ca²⁺ release from vascular smooth muscle cell microsomes. *Exp. Biol. Med. (Maywood)* *227*, 36–44.
- Zhang, J.H., Chung, T.D., and Oldenburg, K.R. (1999). A simple statistical parameter for use in evaluation and validation of high throughput screening assays. *J. Biomol. Screen* *4*, 67–73.
- Zhang, K., Sun, W., Huang, L., Zhu, K., Pei, F., Zhu, L., Wang, Q., Lu, Y., Zhang, H., Jin, H., et al. (2017). Identifying glyceraldehyde 3-phosphate dehydrogenase as a cyclic adenosine diphosphoribose binding protein by photoaffinity protein-ligand labeling approach. *J. Am. Chem. Soc.* *139*, 156–170.

STAR★METHODS

KEY RESOURCES TABLE

REAGENT or RESOURCE	SOURCE	IDENTIFIER
Antibodies		
Cardiac Troponin T Monoclonal Antibody (1C11)	Thermo Fisher Scientific	Cat# MA1-16687
OCT4 antibody	AbCam	Cat# ab18976; RRID:AB_444714
SSEA4 antibody	AbCam	Cat# ab16287; RRID:AB_778073
GAPDH antibody	Cell Signaling Technology	Cat# sc32233; RRID:AB_627679
Goat anti-mouse IgG, Alexa Fluor 488 conjugate	Thermo Fisher Scientific	Cat# A11001; RRID:AB_2534069
anti-mouse IgG, HRP conjugate	Cell Signaling Technology	Cat# 7076; RRID:AB_330924
anti-rabbit IgG, HRP conjugate	Cell Signaling Technology	Cat# 7074; RRID:AB_2099233
Biological samples		
<i>Strongylocentrotus purpuratus</i> egg homogenates	This work	N/A
Sarcoplasmic reticulum vesicles	This work	N/A
Chemicals, peptides, and recombinant proteins		
[3H]-ryanodine	Perkin Elmer	Cat# NET950250UC
Ryanodine	Tocris	Cat# 1329
Hoechst 33342	Thermo Fisher Scientific	Cat# H21492
CHIR	Selleck Chemicals	Cat# 2924
Adenylyl-imidodiphosphate	Sigma Aldrich	Cat# 10102547001
Fluo-4-AM	Thermo Fisher Scientific	Cat# F14201
cADPR	This work, (Walseth and Lee, 1993)	N/A
NAADP	This work, (Jain et al., 2010)	N/A
D-myo-Inositol 1,4,5-tris-phosphate trisodium salt	Sigma Aldrich	Cat# I9766
Creatine kinase	Sigma Aldrich	Cat# C3755
Phosphocreatine	Sigma Aldrich	Cat# P1937
Fluo-3	Biotium	Cat# 50011
Caffeine	Sigma Aldrich	Cat# C0750
FLI-06	Cayman Chemical	Cat# 21272
Tyrphostin AG538	Sigma Aldrich	Cat# 658403
l-O-Me-Tyrphostin AG538	Santa Cruz Biotechnology	Cat# 300821
8NH ₂ -cADPR	This work, (Walseth and Lee, 1993)	N/A
8Br-7CH-cADPR	BioLog	Cat# B 100-005
FLI-06 analog 1 (Table S1)	Chembridge	Cat# 5605456
FLI-06 analog 2 (Table S1)	Chembridge	Cat# 5469731
FLI-06 analog 3 (Table S1)	Chembridge	Cat# 5613161
FLI-06 analog 4 (Table S1)	Chembridge	Cat# 5607743
FLI-06 analog 5 (Table S1)	Chembridge	Cat# 5616720
FLI-06 analog 6 (Table S1)	Chembridge	Cat# 5467399
FLI-06 analog 7 (Table S1)	Chembridge	Cat# 5719662
FLI-06 analog 8 (FLI-28) (Table S1)	Chembridge	Cat# 6874430
FLI-06 analog 9 (Table S1)	Chembridge	Cat# 5857255
FLI-06 analog 10 (Table S1)	Chembridge	Cat# 5136132
FLI-06 analog 11 (Table S1)	Chembridge	Cat# 5607984

(Continued on next page)

Continued

REAGENT or RESOURCE	SOURCE	IDENTIFIER
FLI-06 analog 12 (Table S1)	Chembridge	Cat# 5478865
FLI-06 analog 13 (Table S1)	Chembridge	Cat# 5616033
FLI-06 analog 14 (Table S1)	Chembridge	Cat# 5707932
FLI-06 analog 15 (Table S1)	Chembridge	Cat# 5468595
LOPAC1280	Sigma Aldrich	Cat# LO1280
GPCR Small Molecule Compound Library	Selleck	Cat# L2200-01
Critical commercial assays		
Notch1 Pathway Reporter Kit	BPS Bioscience	Cat# 79503
Experimental models: Cell lines		
iPSCs	Melton laboratory (Dept. of Stem Cell and Regenerative Biology, Harvard)	N/A
U-2 OS	ATCC	Cat# HTB-96
Experimental models: Organisms/strains		
<i>Strongylocentrotus purpuratus</i>	Marinus Scientific	N/A
Recombinant DNA		
pGP-CMV-GCaMP-6M	Chen et al. (2013)	Addgene plasmid # 40754
Software and algorithms		
Origin 2021b	OriginLab	https://www.originlab.com/
Metamorph v7.10	Molecular Devices	https://www.moleculardevices.com/products/cellular-imaging-systems/acquisition-and-analysis-software/metamorph-microscopy#gref

RESOURCE AVAILABILITY**Lead contact**

Further information and requests for resources and reagents should be directed to and will be fulfilled by the lead contact, Jonathan Marchant (jmarchant@mcw.edu).

Materials availability

This study did not generate any new unique reagents.

Data and code availability

All data reported in this paper will be shared by the lead contact upon request.

This paper does not report original code.

Any additional information required to reanalyze the data reported in this paper is available from the lead contact upon request.

EXPERIMENTAL MODEL AND SUBJECT DETAILS**Cell lines**

U2OS cell line (RRID: CVCL_0042). Origin: Human osteosarcoma epithelia.

Culture media and conditions: U2OS cells were obtained from ATCC (Cat# HTB-96) and were cultured in Dulbecco's Modified Eagle's Medium with 10% fetal bovine serum (Thermo Fisher Scientific, Cat# 26140079), penicillin (100 U/ml) and streptomycin (100µg/ml) (Thermo Fisher Scientific, Cat# 15140122) in a humidified 5% CO₂ incubator at 37°C.

Human induced pluripotent stem cells. Origin: iPSCs were generated from dermal fibroblasts from healthy donors by the Melton laboratory (Dept. of Stem Cell and Regenerative Biology, Harvard University).

Culture media and conditions: iPSCs were cultured in Matrigel-coated petri dishes with mTeSR1 (STEM-CELL Technologies, Vancouver, BC, Canada) supplemented with penicillin/streptomycin (Thermo Fisher Scientific) in an incubator (5% CO₂, 21% O₂) at 37°C as previously described (32,51). Culture media was changed daily. iPSCs were digested and passaged at a ratio of 1:6 using Versene (Thermo Fisher Scientific) when they reached 70–80% confluence. MycoAlert® Mycoplasma Detection Kit (Lonza) was used for monitor cultures for mycoplasma.

Cell-free systems

Sea urchin egg homogenates. Origin: Eggs were harvested from live female *Strongylocentrotus purpuratus* specimens, which were collected from the ocean off the coast of Southern California by Marinus Scientific. Gamete secretion was stimulated by injecting specimens with KCl. Eggs were collected, and homogenates were prepared as detailed in the [STAR methods](#) section. Homogenates were aliquoted, flash-frozen, and stored at –80°C.

Sarcoplasmic reticulum vesicles. Origin: Sarcoplasmic reticulum vesicles were isolated from tissues harvested from female porcine which weighed approximately 50kg at time of harvest. Crude sarcoplasmic reticulum (CSR) was isolated from porcine longissimus dorsi muscle and porcine cardiac left ventricle tissue by differential centrifugation of homogenized tissue. Heavy SR (HSR) vesicles, which are enriched in RyR1, were isolated by fractionation of crude skeletal SR vesicles using a discontinuous sucrose gradient. All vesicles were flash-frozen and stored at –80°C.

METHOD DETAILS

Drugs and molecular reagents

Chemical reagents were sourced as follows: fluo-4 AM (Thermo Fisher); fluo-3 pentapotassium salt (Biotium). HEPES, CHAPS, potassium gluconate, N-methylglucamine, ATP, and DTT (Sigma Aldrich); cOmplete™ EDTA-free protease inhibitor cocktail (Roche); ryanodine (Enzo Life Sciences); . FLI-06 (cyclohexyl 2,7,7-trimethyl-4-(4-nitrophenyl)-5-oxo-1,4,5,6,7,8-hexahydroquinoline-3-carboxylate, C₂₅H₃₀N₂O₅), tyrphostin AG538 (AG538, α -Cyano-(3,4-dihydroxy)cinnamoyl-(3',4'-dihydroxyphenyl)ketone, C₁₆H₁₁O₅) and I-O-Me-Tyrphostin AG538 (I-O-Me-AG538, α -Cyano-(3-methoxy-4-hydroxy-5-iodocinnamoyl)-(3',4'-dihydroxyphenyl)ketone, C₁₇H₁₂INO₅) were purchased from Cayman Chemical, Sigma Aldrich, and Santa Cruz Biotechnology respectively. Caffeine and IP₃ were purchased from Sigma Aldrich. cADPR, 8-NH₂-cADPR, and NAADP were synthesized in house using previously detailed [STAR methods](#) (Jain et al., 2010; Walseth and Lee, 1993). Drug libraries used for the sea urchin screen were from Sigma (LOPAC®¹²⁸⁰, Library of Pharmacologically Active Compounds, 1280 compounds) and Selleck (GPCR compound library, 254 compounds). FLI-06 analogs were sourced from ChemBridge. A Human Notch1 reporter assay (BPS Bioscience) was used per manufacturer's instructions.

Chemical syntheses

cADPR was synthesized by incubating NAD⁺ (Sigma Aldrich) with *Aplysia* ADP-ribosyl cyclase. The resulting cADPR was purified by HPLC on an AG MP-1 column. 8-NH₂-cADPR was synthesized as follows: 8-azido-AMP (Sigma Aldrich) was converted to 8-amino-AMP in the presence of 15mM dithiothreitol, and purified on a MONO Q HR column. 8-amino-AMP (0.1 μ mol), β -NMN (0.1 μ mol, Sigma Aldrich) and MgCl₂ (2 μ mol) were combined in a microfuge tube and evaporated to dryness using a Speedvac concentrator. A coupling reaction was initiated by adding 20 μ L of 1.5 M HEPES-NaOH (pH 6.8) and 20 μ L of 1.5 M 1-ethyl-3-(3-dimethyl-aminopropyl)- carbodiimide-HCl (EDC) and incubated at 37°C for 12 to 18 h. The resulting 8-amino-NAD⁺ was purified by HPLC on an AG MP-1 column. 8-amino-NAD⁺ was converted to 8-amino-cADPR using *Aplysia* ADP-ribosyl cyclase as previously described [35]. The 8-amino-NAD⁺ was incubated for 2 to 4 h at room temperature with ADP-ribosyl cyclase. The resulting 8-amino-cADPR was purified by HPLC on an AG MP-1 column as described above. NAADP was synthesized by incubating nicotinamide adenine dinucleotide phosphate (NADP, Sigma-Aldrich) with nicotinic acid in the presence of recombinant *Aplysia* ADP-ribosyl cyclase (47) and purified by high-performance liquid chromatography (HPLC). All purified compounds were evaporated to dryness on a SpeedVac concentrator and stored at –20°C.

Ca²⁺ flux assays in sea urchin egg homogenate

Strongylocentrotus purpuratus specimens were sourced from Marinus Scientific. *S. purpuratus* egg homogenates (25%) were prepared as detailed previously (Clapper et al., 1987) and stored at -80°C . Briefly, *S. purpuratus* specimens were injected with 1 mL of 0.5M KCl into each coelomic cavity to stimulate gamete shedding. Eggs were collected by inverting female specimens and placing them onto beakers containing artificial sea water (ASW). Eggs were pooled, gently washed in artificial sea water, and dejellied via filtration through a 100 μm nylon mesh. Eggs were washed in once with Ca²⁺-free ASW supplemented with 1 mM EGTA to remove extracellular Ca²⁺, and were washed two more times with Ca²⁺-free ASW to remove residual EGTA, centrifuging samples at 100 x RCF for 2 min at 4 $^{\circ}\text{C}$ between washes. Eggs were finally washed twice with potassium gluconate intracellular medium (K-GluIM) (250mM NMDG, 250mM K-gluconate, 20mM HEPES, 1mM MgCl₂, pH 7.2). Eggs were centrifuged supernatant was aspirated, and packed eggs were suspended in 3 volumes of K-GluIM supplemented with 2mM MgATP, 20mM phosphocreatine, 20 U/ml creatine phosphokinase, and cOmplete EDTA-free protease inhibitor cocktail (Roche). Suspended eggs were homogenized in a tight fitting Dounce homogenizer. Homogenized samples were aliquoted, flash-frozen, and stored at -80°C until use. For experiments, homogenates were loaded with Ca²⁺ and fluo-3 by incubation at 17 $^{\circ}\text{C}$ in intracellular-like medium (250mM potassium gluconate, 250mM N-methyl-D-glucamine, 20mM HEPES, 1mM MgCl₂, pH 7.2, supplemented with 0.3mg/mL creatine kinase, 0.5mM ATP, 4 mM phosphocreatine, and 3 μM Fluo-3 (Walseth et al., 2012)). The homogenate was diluted in a step-wise fashion to a final concentration of 1.25% homogenate over a period of 3 h. Calcium dynamics were monitored by following fluo-3 fluorescence using a Tecan Infinite M1000 Pro plate reader ($\lambda_{\text{ex}} = 485 \pm 5\text{nm}$, $\lambda_{\text{em}} = 525 \pm 5\text{nm}$). Baseline fluorescence readings from samples in the presence of individual drugs were resolved, followed by stimulation with cADPR. Drug screening was performed in 96-well assay plates (Corning #3590 flat bottom, transparent) at a final concentration of 25 μM . An epMotion® 96 liquid handling workstation (Eppendorf) was used to dispense homogenate and ligands into assay plates. Fluo-3 fluorescence was monitored in the presence of compound for 35 cycles (6 min) prior to the addition of an EC₇₀ concentration of cADPR (300nM final concentration). For the LOPAC^{®1280} library, 0.25 μL of vehicle (DMSO) or compound (10mM) was dispensed into the assay plates using a LabCyte ECH0550 acoustic nanoliter dispensing system. The assay was started by addition of 99.75 μL of sea urchin egg homogenate. For screening the Selleck GPCR compound library, baseline fluo-3 fluorescence of the homogenate (97.5 μL) was monitored for 90 s prior to the addition of 2.5 μL vehicle (DMSO) or compound (1mM) using the epMotion®96. For the LOPAC^{®1280} library, all drugs were screened in singlicate. For the GPCR library, compounds were screened in duplicate. Z' factor for both vehicle control and cADPR responses was calculated as follows: $Z' = 1 - (3(\text{stdev}_{\text{max}} + \text{stdev}_{\text{min}})/(\text{mean}_{\text{max}} - \text{mean}_{\text{min}}))$.

Mammalian cell microinjection

Human U2OS cells (bone osteosarcoma) were transfected with a plasmid encoding the genetically-encoded Ca²⁺ indicator GCaMP-6M (Chen et al., 2013) two days prior to microinjection assays. Transfection was performed using Lipofectamine 3000 (Thermo Fisher Scientific) in accordance with the vendor's protocol. One day following transfection, 1x10⁶ cells were seeded onto collagen coated MatTek dishes. For microinjection experiments, dishes were mounted on an Olympus IX81 inverted microscope equipped with a piezo nano-positioning stage (Prior Scientific). Cells were perfused with Ca²⁺-free Hank's Balanced Salt Solution (Thermo Scientific) at a rate of 0.5 mL/min. Isolated U2OS cells expressing GCaMP6M identified by fluorescence were selected for injections. Cell morphology was assessed by acquiring z-stack images and reconstructing three-dimensional models of each cell to be injected. Regions that were not relatively close to the nucleus or cell periphery were targeted for injection sites. Femtotip (Eppendorf) injection pipettes were backfilled with intracellular buffer (110mM KCl, 10mM NaCl, 20mM HEPES, pH 7.2) containing either vehicle or cADPR (30 μM) and positioned using an Injectman-4 (Eppendorf) micromanipulation system. Cells were injected at a z-position approximately 70% of the cell thickness using a Femtojet4i (Eppendorf). Injection parameters were 85hPa injection pressure, 40hPa compensation pressure, 0.5s injection duration, 45 $^{\circ}$ injection angle, and 600 $\mu\text{m/s}$ injection speed. Cells were imaged ($\lambda_{\text{ex}} = 488\text{nm}$, $\lambda_{\text{em}} = 514 \pm 15\text{nm}$ band-pass) using a Plan-Apochromat 60x/1.42 objective, and fluorescence changes were monitored using a Yokogawa spinning disk confocal (CSU-X- M1N) and an Andor iXon Ultra 888 EMCCD camera. Image acquisition and data analysis was performed using Metamorph (version 7.10).

[³H]-ryanodine binding to SR vesicles

[³H]-ryanodine binding assays were performed as outlined previously (Fruen et al., 2000). Briefly, in 96-well plates, HSR vesicles (1 mg/mL) and cardiac CSR vesicles (3mg/mL) were incubated with 0.02% DMSO or

compound (concentration indicated) for 3hr at 37°C in a solution containing 150mM KCl, 0.1µM calmodulin, 5 mM GSH, 2mM dithiothreitol, 1 µg/mL Aprotinin and Leupeptin, 1 mM EGTA, 238µM or 1.62mM CaCl₂ (as determined by MaxChelator to yield 100 nM or 30 µM of free Ca²⁺, respectively), 0.1 mg/mL BSA, [³H]-ryanodine (7.5 and 10nM for cardiac and skeletal SR, respectively) and 20mM K-PIPES (pH 7.0). Non-specific and maximal [³H]-ryanodine binding to SR were separately assessed by addition of 40µM non-radioactively labeled ryanodine or 5mM Adenylyl-imidodiphosphate, respectively. Such control samples were each distributed over 4 wells/plate. After incubation, unbound [³H]-ryanodine was removed by filtration through grade GF/B Glass Microfiber filters (Brandel Inc., Gaithersburg, MD) using a 96-sample Brandel Harvester. In 4mL of Ecolite Scintillation cocktail (MP biomedical, Solon, OH, USA), Radioactivity on the filter was counted using a Beckman LS6000 scintillation counter (Fullerton, CA). All experiments were run with 3 different batches of SR. Statistical analysis was performed using a two-way, unpaired Student's T-test.

Human iPSC culture and cardiomyocyte differentiation. Prior to the initiation of CM differentiation, iPSCs were digested with 3 mL Accutase (Innovative Cell Technologies) for 5 min to yield single cells. Digested cells were counted by a Cellometer (Nexcelom Bioscience), and plated (1.76x10⁶/well) on a Matrigel-coated 6-well plate, and cultured with mTeSR1 medium. The following day, the medium was replaced with fresh mTeSR1. This time point was defined as day '-2'. Culture medium was changed daily. CM differentiation from iPSCs was conducted by temporal modulation of Wnt signaling (Horikoshi et al., 2019; Kikuchi et al., 2015; Lian et al., 2012). At day '0', when iPSCs reached over 95% confluence, CM differentiation was started. iPSCs were cultured with Roswell Park Memorial Institute (RPMI)/B-27 Supplement Minus Insulin (Thermo Fisher Scientific) with 12µM CHIR (GSK-3 inhibitor, Selleck Chemicals) and 1% penicillin/streptomycin (Thermo Fisher Scientific) in a normoxic incubator (20% O₂, 5% CO₂). Twenty-three hours after administration of CHIR, the medium was replaced with RPMI/B27 Minus Insulin and changed daily. At day '3', around 72 h after administration of CHIR, the medium was replaced by fresh RPMI/B27 Minus Insulin/5µM IWP-4 (Wnt/beta-catenin inhibitor, Stemgent) and the cells were cultured for 48 h. At day 5, the medium was replaced with RPMI/B27 Minus insulin, changed every two days. The RPMI medium supplemented with B27 Supplement (with insulin) was used continually for cell culture from day '6'. Cultures were observed daily under the microscope. To determine the effect of FLI-06 (prepared as 10 mM stock solution in DMSO) on the CM differentiation, iPSCs were treated at day '0' with 1µM FLI-06 or an equal volume of DMSO as a vehicle control for either 23 h or 5 days.

Immunofluorescence staining. CMs cultured on Matrigel-coated coverslips were fixed with 4% paraformaldehyde (Electron Microscopy Sciences) for 15 min at room temperature, permeabilized with 0.5% Triton X-100 (Sigma-Aldrich) for 15 min, and blocked with 10% donkey serum (Millipore) for 20 min at room temperature as previously described (Kikuchi et al., 2015). Cells were then incubated in a moist chamber (overnight, 4°C) with primary antibody to detect cardiac troponin T (1:200 dilution; MA1-16687 Thermo Fisher Scientific). After washing with PBS twice, cells were incubated in the dark (1 h, 37°C) with a secondary antibody (Alexa Fluor 488 goat anti-mouse IgG, 1:1000, Thermo Fisher Scientific). Hoechst 33342 (Thermo Fisher Scientific) was used to stain nuclei. CM differentiation efficiency was quantified by counting the number of troponin T-positive CMs in the field versus total cell nuclei.

Western blotting. CMs were lysed on ice with RIPA lysis buffer (Cell Signaling Technology) in the presence of phenylmethylsulfonyl fluoride (Sigma-Aldrich) and phosphatase inhibitor tablets (Roche). Protein samples were boiled (5 min) and 20 µg of total protein loaded for Western analysis. Blots were incubated (overnight on rocker, 4°C) with mouse anti-cardiac troponin T (Thermo Fisher Scientific) or rabbit anti-GAPDH (glyceraldehyde-3-phosphate dehydrogenase; Cell Signaling Technology). Primary antibodies were washed out with Tris-buffered saline containing supplemented with 0.1% Tween-20. Membranes were incubated with secondary antibodies conjugated to horseradish peroxidase (Cell Signaling, 1 h at room temperature). Proteins were detected using ECL Prime Western Blotting Reagents (GE Healthcare) and imaged using a ChemiDoc MP imaging system (Bio-Rad). Signal intensity was quantified by normalization to GAPDH and presented as a percentage of vehicle control-treated CMs.

QUANTIFICATION AND STATISTICAL ANALYSIS

Fluorescence traces in Figure 1A are representative traces from 15 individual wells per condition while screening chemical libraries. Traces in Figures 2A,2C and 2E represent mean ± s.e.m. changes in fluo-3 fluorescence across three individual wells per condition from a single experiment. Curves in Figures 2B,2D,2F,2G,2H,2I and 2J represent mean ± s.e.m. values from three independent biological experiments,

with three technical replicates per condition in each experiment. IC_{50} values were calculated from curves depicted in Figures 2B,2D and 2F, using OriginLab logistic fit. Traces in Figure 3B and bar graph values in Figures 3C and 3D represent mean \pm stdev changes in GCaMP6M fluorescence from three independent microinjection experiments per condition. Quantification of area under the curve in Figure 3D was accomplished using the OriginLab curve integration function. Traces in Figure 4A represent fluo-3 fluorescence values from 4 individual wells per condition from a single representative experiment. Curves in Figure 4B represent mean \pm s.e.m. fluo-3 fluorescence values from three independent biological experiments, with four technical replicates per condition in each experiment. Data in Figure 4C represent mean \pm s.e.m. [3H]-ryanodine binding relative to DMSO controls from three separate biological replicates, each run with three technical replicates per experiment. Data in Figure 5C represents mean \pm stdev percent of troponin T-positive cells from three independent biological experiments. Data in Figure 5D represents mean \pm stdev expression of troponin T, relative to GAPDH, from three independent biological experiments. Data in Figure 6 represent relative inhibition of Notch signaling, as well as IC_{50} values for inhibition of cADPR-evoked Ca^{2+} release. Inhibition of Notch signaling is determined from three independent biological experiments. IC_{50} values in Figure 6 were derived from three independent biological experiments, with two technical replicates per condition, and were calculated using OriginLab logistic fit. Statistical analyses were conducted using the Student's t-test. p values less than 0.05 was considered statistically significant and the levels are indicated as: *p < 0.05, **p < 0.01.